

View Article Online
View Journal

ChemComm

Chemical Communications

Accepted Manuscript

This article can be cited before page numbers have been issued, to do this please use: V. Fernández-Moreira, E. Morales-Pioz, M. Redrado, A. Benedí Visiedo, A. de Aquino, P. García-Orduña, M. Royo-Cañas, J. Godino, I. Marzo, L. Rodriguez and M. C. Gimeno, *Chem. Commun.*, 2025, DOI: 10.1039/D5CC04768D.



This is an Accepted Manuscript, which has been through the Royal Society of Chemistry peer review process and has been accepted for publication.

Accepted Manuscripts are published online shortly after acceptance, before technical editing, formatting and proof reading. Using this free service, authors can make their results available to the community, in citable form, before we publish the edited article. We will replace this Accepted Manuscript with the edited and formatted Advance Article as soon as it is available.

You can find more information about Accepted Manuscripts in the <u>Information for Authors</u>.

Please note that technical editing may introduce minor changes to the text and/or graphics, which may alter content. The journal's standard <u>Terms & Conditions</u> and the <u>Ethical guidelines</u> still apply. In no event shall the Royal Society of Chemistry be held responsible for any errors or omissions in this Accepted Manuscript or any consequences arising from the use of any information it contains.



Open Access Article. Published on 05 2025. Downloaded on 07/11/25 03:18:40.

No This article is licensed under a Creative Commons Attribution-NonCommercial 3.0 Unported Licence

View Article Online DOI: 10.1039/D5CC04768D

COMMUNICATION

Cyclometallated Iridium(III) Complexes: Ligand-Driven Selectivity for Chemotherapy and Photodynamic Therapy

Received 00th January 20xx, Accepted 00th January 20xx

DOI: 10.1039/x0xx000000x

Eva Morales-Pioz^a, Marta Redrado^b, Andrea Benedi^a, Araceli de Aquino^c, Pilar García-Orduña^a, María Royo-Cañas^d, Javier Godino^e, I. Marzo,^f Laura Rodríguez^c, M. Concepción Gimeno^a* and Vanesa Fernández-Moreira^a*

This study explores two cyclometallated Ir(III) complex families with distinct therapeutic profiles. Benzothiophene derivatives (1, 2) exhibit potent antiproliferative character in the dark, favoring chemotherapy, while benzothiazole analogs (3 and 4) show high photocytotoxicity, ideal for photodynamic therapy. Photophysical studies and subcellular localization analyses highlight ligand-driven selectivity and the role of organelle targeting in therapeutic outcomes.

Chemotherapy and photodynamic therapy (PDT) are key cancer treatments where metallodrugs have shown great potential. Since cisplatin's anticancer properties discovery in 1965, several Pt(II), Ru(II), Au(I), As(I), and Fe(II) compounds have reached clinical use.1 Improving selectivity and potency remains central, often through rational ligand design. Although PDT's clinical adoption was initially limited by technology, recent advances like TOOKAD® (Pd(II) porphyrin) and TLD1433 (Ru(II) complex)² have promoted the interest in metal-based photosensitizers.^{3,4} Traditional tetrapyrrolic photosensitizers face limitations in solubility, stability, and synthetic accessibility, whereas d⁶ metal complexes, particularly Ir(III) compounds, offer tunable photophysical properties, efficient singlet oxygen generation, and deep tissue penetration, making them promising candidates for PDT applications.5,6 For example, Gasser and Chao reported mitochondrial-targeting Ir(III) photosensitizers that induce immunogenic cell death,7 while Brabec⁸ and Mao⁹ described complexes targeting mitochondrial DNA or damaging lysosomes, respectively. Additionally, Espino and Massager developed β -carboline-based Ir(III) photosensitizers with high selectivity against prostate cancer cells.¹⁰

Despite recent advances, achieving predictable therapeutic selectivity remains challenging due to the complexity of the tumor microenvironment, including oxidative stress, pH, and cellular heterogeneity.11 In fact we previously reported pyrazole-based Ir(III) complexes showing cell-line-dependent both chemotherapeutic agents photosensitizers, highlighting the need for deeper mechanistic understanding. 12 To further explore how ligand design influences therapeutic outcomes, investigated $[Ir(C^N)_2(N^N)]^+$ complexes bearing either pyridylbenzothiophene (Py-Btp) or 2-phenylbenzothiazole (Ph-Btz) as C^N ligands (Fig. 1), chosen for their oxygen-sensitive emission and promising PDT potential. 13,14 In this study, we in evaluate their performance combination benzimidazole-based N^N ligands for selective chemotherapy and PDT. Complexes 1-4 were synthesized as shown in Fig. S1 (ESI+) and fully characterized by ¹H and ¹³C NMR (including COSY, HSQC, and HMBC), HRMS, and elemental analysis (Fig. S2-S27, ESI+). Additional X-Ray diffraction of complex 3 supports the given octahedral connectivity, Fig. 2a, S28 and Table S1.

[†] Electronic Supplementary Information (ESI) available: Synthetic procedures, characterisation data, methodology, supporting figures and tables. CCDC 2405786. For ESI and crystallographic data in CIF or other electronic format see DOI: 10.1039/x0xx00000x

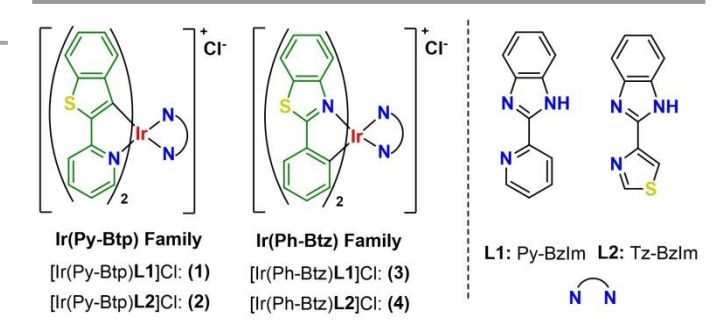


Fig. 1. Structures of complexes 1-4.

a-Instituto de Síntesis Química y Catálisis Homogénea (ISQCH), CSIC-Universidad de Zaragoza, Pedro Cerbuna 12, 50009 Zaragoza, Spain. gimeno@unizar.es, vanesa@unizar.es

b. Chimie ParisTech, PSL University, CNRS, Institute of Chemistry for Life and Health Sciences, Laboratory for Inorganic Chemical Biology, 75005 Paris, France.

Departament de Química Inorgànica i Orgànica, Secció de Química Inorgànica,
 Universitat de Barcelona, Martí i Franquès 1-11, 08028 Barcelona, Spain.

d Servicio Científico-Técnico de Microscopía e Imagen, Instituto Aragonés de Ciencias de la Salud, 50009 Zaragoza, Spain.

e Servicio Científico-Técnico de Separación Celular y Citometría, Instituto Aragonés de Ciencias de la Salud, 50009 Zaragoza, Spain.

f- Departamento de Bioquímica y Biología Molecular, Universidad de Zaragoza, 50009 Zaragoza, Spain.

This article is licensed under a Creative Commons Attribution-NonCommercial 3.0 Unported Licence

Open Access Article. Published on 05 2025. Downloaded on 07/11/25 03:18:40.

Journal Name COMMUNICATION

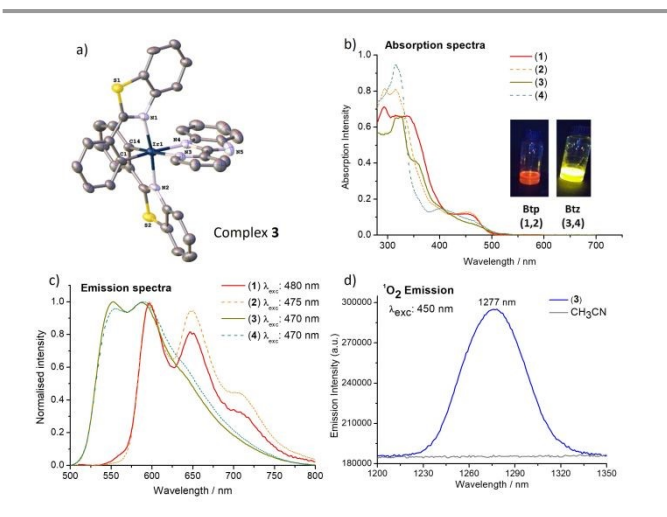


Fig. 2. (a) Molecular structure of cationic complex 3 (H atoms omitted for clarity). (b) Absorption and (c) emission spectra of 1-4 in DMSO (5×10⁻⁵ M). (d) Singlet oxygen generation by 3 in CH₃CN (5×10⁻⁵ M) upon 450 nm excitation.

Complexes 1-4 exhibited characteristic absorption features, with intense LC $(\pi \rightarrow \pi^*)$ bands between 293–350 nm ($\epsilon \approx$ 33,000-40,000 M⁻¹cm⁻¹) and weaker MLCT bands in the 400-464 nm range (Fig. 2b). 15 The absorption tails beyond 500 nm suggest contributions from triplet MLCT and/or LC states. UV-Vis spectra after 48 h in DMSO and PBS:DMSO (9:1) confirmed good stability (Fig. S30-S33). Upon irradiation, all complexes showed phosphorescence in fluid solution (DMSO and CH₃CN) at 298 K (Fig. S34-S43), with emission spectra presented in Fig. 2c and S44-S47 and summarized in Table 1 and S2 (ESI+). Structured emission was observed for benzothiophene-based complexes 1 and 2 (λ em = 595–598 nm, with tails >750 nm), consistent with a $^3LC(C^N, \pi \rightarrow \pi^*)$ character. ¹⁶ In contrast, benzothiazole analogues 3 and 4 emitted near 570 nm with unstructured profiles, indicative of enhanced MLCT($(d\pi(Ir)\rightarrow\pi^*(N^N))/LLCT(\pi(C^N)\rightarrow\pi^*(N^N))$ mixing.¹⁷ In aerated solution emission lifetimes were shorter in CH₃CN than in DMSO due to oxygen quenching (Fig. S34-S43). Accordingly, quantum yields increased in deoxygenated DMSO, reaching 38% (1 and 2), and 83% (3 and 4).

Table 1. Photophysical data of 1 - 4 measured in DMSO and/or CH₃CN solution at 298 K

	$\lambda_{\text{em}}/\text{nm}$ $(\lambda_{\text{exc}}/\text{nm})^{[a]}$	λem/nm (λexc/nm) ^[b]	τ/μs ^[a]	τ/μs ^[b] (τ/μs ^[d])	$\Phi_{em}^{[a]}$ $(\Phi_{em}^{[c]})$	Φ _Δ (¹O ₂) ^[b]
1	597, 649,	592, 642,	1.71	0.19	0.02	0.44
	706 (480)	703 (475)		(4.52)	(0.38)	
2	597, 649,	590, 642,	3.47	0.20	0.02	0.44
	706 (475)	700 (450)		(4.92)	(0.38)	
3	552, 587,	530, 572,	1.86	0.27	0.16	0.55
	637 (470)	617 (425)			(0.83)	
4	555, 590,	541, 567	0.89	0.23	0.15	0.50
	640 (470)	(425)			(0.82)	

Note: Emission (λ em), lifetimes of excited state (τ), emission quantum yields (Φ) and 1O_2 generation quantum yield (1O_2 , \emptyset) of compounds 1-4 in (2×10⁻⁵ M) in DMSO or CH₃CN solutions at 298K. [a] Aerated DMSO solution. [b] Aerated CH₃CN solution. [c] N₂ saturated DMSO solution. [d] N₂ saturated CH₃CN solution.

Singlet oxygen generation was confirmed by emission at 1272 nm under 450 nm excitation in aerated @H3@AP (Fig.526),4548D S50), with no signal in neat solvent, excluding artefacts. Using perinaphthenone as a reference, ¹O₂ quantum yields ranged from 44-55%, highlighting the strong photosensitizing potential of all complexes for PDT.

The antiproliferative activity of Ir(III) complexes 1-4 was analysed in A549 (lung) and HeLa (cervical) cancer cells, in the dark and under irradiation, Table 2. Upon light exposure, all complexes exhibited enhanced antiproliferative effect, probably related to ¹O₂ generation. In A549 cells, lightactivated IC₅₀ values were \leq 0.34 μ M. In the dark, Btp complexes 1 and 2 were active (IC₅₀ \approx 1 μ M), while Btz analogues 3 and 4 were far less (IC₅₀ ≈ 100 µM), making them more suitable for PDT. In HeLa cells, all complexes showed low micromolar IC₅o values regardless of light, indicating selective PDT activity of 3 and 4 in A549 cells. Control ligands (Py-BzIm, Tz-BzIm) were inactive, and cisplatin showed antiproliferative activity consistent with published data.18

Given their strong PDT performance in A549 cells (PI = 291 for 3, 1054 for 4) and the chemotherapeutic potential of 1 and 2, further biological analyses were conducted on representative complexes from each family. LogP measurements revealed slightly higher lipophilicity for 1 and 2, which could influence uptake. However, ICP-MS analysis showed similar cellular accumulation of 1 and 3 (200.9 \pm 56 and 186.3 \pm 37 (ng/ml) / 106 cells), suggesting that differences in their antitumor activity are not solely due to uptake (Fig. S51a).

Cell death mechanism was assessed by Annexin V and PI staining and flow cytometry, and dose-dependent apoptosis was confirmed under light exposure (Fig. 3a,b). Complex 3 triggered significant cell death even at low doses (~90% at 2×IC₅₀; Fig. 3b-left). In contrast, complex 1 toxicity was moderate at this range (~30% cell death at 2×IC₅₀) and was enhanced with increasing dose (~70% cell death at 4×IC₅o).

Table 2. IC₅₀ values (µM) of compounds 1-4. Pv-BzIm. Tz-BzIm and cisplatin incubated with A549 and HeLa. LogP values of complexes 1-4.

	A549	A549	HeLa	HeLa	LogP
	IC ₅₀ (DARK)	PI	IC ₅₀ (DARK)	PI	
	(IC ₅₀ (Irr.))		(IC ₅₀ (Irr.))		
1 ^[a]	0.99 ± 0.24	66	1.76 ± 1.01	176	1.59
	(0.015 ± 0.002)		(0.010 ± 0.005)		
2 ^[a]	0.65 ± 0.12	38	0.70 ± 0.60	70	2.49
	(0.017 ± 0.003)		(0.010 ± 0.003)		
3 ^[a]	99 ± 1.30	291	> 5	-	1.47
	(0.34 ± 0.02)		(0.030 ± 0.022)		
4 ^[a]	116 ± 1.10	1054	1.50 ± 0.70	150	1.63
	(0.11 ± 0.02)		(0.010 ± 0.001)		
Py-BzIm ^[b]	> 100	-	68.50 ± 0.90	-	n.d.
	n.d.		n.d.		
Tz-Bzlm ^[b]	> 100	-	> 100	-	n.d.
	n.d.		n.d.		
Cisplatin ^[b]	9.39 ±0.08		8.05 ± 0.13	-	n.d.

[a] Conditions: 48 h incubation in the dark and under irradiation (470 nm, 10 min, 1.6 J/cm²). PI = IC $_{50}$ (dark)/IC $_{50}$ (light). [b] Conditions: 48 h incubation in the dark only, as these compounds are not light-activatable. LogP values from the shakeflask method.19 n.d.: not determined.

This article is licensed under a Creative Commons Attribution-NonCommercial 3.0 Unported Licence

Open Access Article. Published on 05 2025. Downloaded on 07/11/25 03:18:40.

Journal Name

Under dark conditions, only complex 1 was evaluated, as complex **3** exhibited a high IC₅₀ value (99 \pm 1.3 μ M). Complex **1** showed a modest cytotoxic effect even at the highest concentration tested (~30% cell death at 13.7×IC₅₀ Fig. 3bright), suggesting a distinct mechanism of action in the dark and upon irradiation (Fig. S51b). Moreover, cell cycle analysis showed that complex 1 inhibited cell proliferation under both dark and irradiated conditions, producing only minor alterations in the G0/G1 and G2/M phases. These results suggest a cytostatic effect at low doses in both cases (Fig. 3c and S51c-d). However, complex 3 (IC₅₀) induced G0/G1 arrest in the dark (Fig. S51c). Furthermore, complex 1 and 3 induced dose-dependent intracellular ROS generation in the dark and under irradiation respectively (Fig. S51e) consistent with previous reports on similar Ir(III) complexes.²⁰ These results suggest that both complexes induce light-triggered apoptosis, particularly potent in the case of complex 3. In fact, complex 1 at concentrations close to the IC_{50} would exert a cytostatic effect after irradiation, and this effect also predominates in darkness. Subcellular localization is known to play a critical role in the therapeutic efficacy and selectivity of metallodrugs. To better understand the differing therapeutic outcomes of the two Ir(III) families, the intracellular distribution of complexes 1-4 was examined in A549 cells using confocal microscopy. Mitochondria were stained with MitoTracker Deep Red (MTDR). All complexes were internalized by the cells and did not accumulate in the nucleus. Notably, complexes 1 and 2 predominantly localized to mitochondria, as indicated by strong colocalization with MTDR (Pearson coefficients: 0.78 and 0.62, respectively). This mitochondrial accumulation likely contributes to their higher antiproliferative activity in the dark, given the central role of mitochondria in cellular function. In contrast, complexes 3 and 4 showed poor mitochondrial localization (Pearson coefficients < 0.35), which may explain their reduced dark activity (Fig. 4 and S52). These observations are consistent with the organelle's pivotal role in energy production and survival of cells²¹ and with prior studies reporting enhanced biological activity in iridium complexes engineered for mitochondrial targeting.¹³

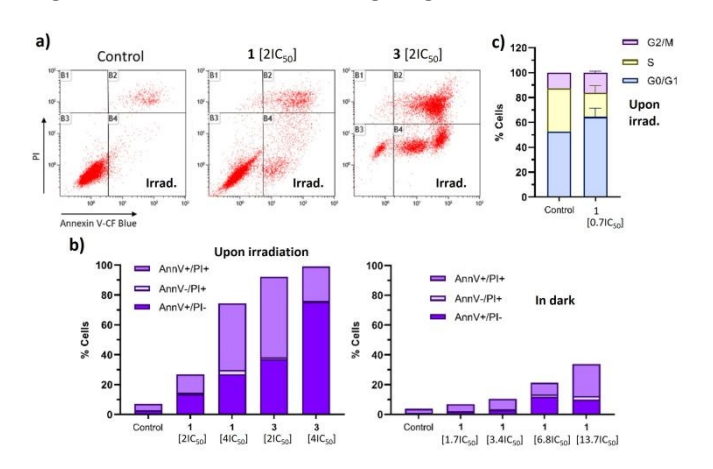
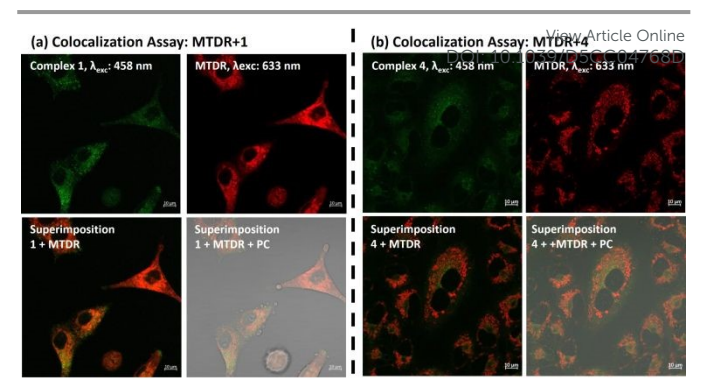


Fig. 3 (a) Dot plots showing A549 cell death after 48 h incubation with **1** and **3**, followed by 470 nm irradiation (10 min, 1.6 J/cm²) using Annexin V-CF Blue/PI staining. (b) Cell death induced by **1** and **3** under light and dark conditions. (c) Cell cycle distribution for compound **1** at the indicated dose post-irradiation.



COMMUNICATION

Fig. 4 (a) Confocal images of A549 cells incubated with complex $\bf 1$ (6 μ M, 2 h), then stained with MitoTracker Deep Red (MTDR, 100 nM, 30 min). (b) Same for complex $\bf 4$. Excitation: 458 nm ($\bf 1$ and $\bf 4$), 633 nm (MTDR). Emission: 552–623 nm ($\bf 1$ and $\bf 4$), 638–755 nm (MTDR). PC: phase contrast.

To further confirm the higher mitochondrial accumulation of the benzothiophene-based complex (1) compared to its benzothiazole counterpart (3), mitochondrial Ir content was quantified by ICP-MS, Fig S53. Complex 1 showed greater uptake (5.52 ng/10⁶ cells) than complex 3 (3.65 ng/10⁶ cells), likely due to its higher logP value. This aligns with the negatively charged mitochondrial membrane favoring the accumulation of lipophilic, cationic species like complex 1.²¹ To investigate possible lysosomal localization, additional colocalization assays were performed using LysoTracker Deep

colocalization assays were performed using LysoTracker Deep Red (LTDR). While LTDR showed strong fluorescence in control conditions, its signal disappeared when co-incubated with any of the Ir complexes (Fig. S54), suggesting fluorescence quenching, likely due to singlet oxygen generated upon light activation. This is in line with previous studies reporting singlet oxygen-mediated quenching of fluorescent dyes such as LysoTracker by Danglot and Collot.²² To determine if this quenching was specific to LTDR, LysoTracker Green (LTG) and LysoTracker Red (LTR) were also tested. Both dyes displayed fluorescence in control cells but were quenched in the presence of the Ir complexes, supporting lysosomal localization and the potential involvement of singlet oxygen in dye quenching (Fig. S55). However, cell-free fluorescence studies under controlled conditions failed to reproduce the quenching effect, suggesting that it may be specific to the cellular environment.

Overall, the colocalization assays indicate that complexes **1**–4 localize to both mitochondria and lysosomes. Complexes **1** and **2**, which bear benzothiophene ligands, exhibit greater mitochondrial accumulation than their benzothiazole analogues (complexes **3** and **4**), a feature that may underlie their higher antiproliferative activity under dark conditions. At first glance, this seems counterintuitive, since mitochondrial dysfunction is typically associated with apoptosis,²¹ yet complexes **3** and **4**, which show lower mitochondrial accumulation, are the ones inducing apoptotic cell death.

To resolve this apparent discrepancy, mitochondrial membrane potential (MMP) was assessed by flow cytometry. As shown in Fig. 5a, complex **3** caused a pronounced loss of MMP following irradiation, consistent with mitochondrial damage and apoptosis.

This article is licensed under a Creative Commons Attribution-NonCommercial 3.0 Unported Licence

2025. Downloaded on 07/11/25 03:18:40.

Open Access Article. Published on 05

60

Fig.5 (a) Percentage of A549 cells with disrupted mitochondrial membrane potential after treatment with complexes 1 and 3, in the dark and postirradiation (470 nm, 10 min, 1.6 J/cm²). *p<0.05; **p<0.01; ***p<0.001. (b) Morphology and viability of A549 spheroids after 6 days of treatment with complexes $\boldsymbol{1}$ and $\boldsymbol{3}$ at their IC50 values (dark conditions). Scale bar: 50 $\mu m.$

In contrast, complex 1 had minimal impact on MMP, both in the dark and under irradiation, with only a slight decrease observed at higher doses. These findings support the previously observed cytostatic profile of complex ${\bf 1}$ under both conditions, while highlighting the photoactivated cytotoxic nature of complex 3, driven by significant mitochondrial impairment. Finally, 3D multicellular tumor spheroids (MCTSs) were used to mimic in vivo tumor conditions. Treatment of A549 MCTSs with complex 1 led to significant inhibition of growth after six days, outperforming both complex 3 and cisplatin, Fig. 5b S56-57. This supports the higher antitumor activity in dark of complex 1 in both 2D and 3D models and underscores its promise for chemotherapeutic therapy via a cytostatic pathway.

This study presents two families of cyclometallated Ir(III) complexes with distinct therapeutic profiles governed by ligand structure. Benzothiophene-based complexes (1 and 2) showed potent antiproliferative activity in the dark, consistent with a cytostatic mechanism and mitochondrial accumulation, making them promising chemotherapeutic agents. However, at high concentrations, an apoptotic cell death pattern is under observed specially irradiation. In benzothiazole-based complexes (3 and 4) exhibited strong photocytotoxicity and induced apoptosis upon light activation even at low concentrations, correlating with mitochondrial dysfunction and singlet oxygen generation, positioning them as effective photosensitizers for PDT. Notably, complexes 3 and 4 displayed marked cell-line selectivity, showing higher PDT activity in A549 than in HeLa cells, indicating a differential therapeutic response depending on the cancer type. Subcellular localization, cell death mechanism, and activity in 3D spheroids further support ligand-driven selectivity. These findings highlight the potential of rational ligand design in tuning the mode of action and selectivity of metal-based anticancer agents.

This work was supported by projects PID2022-137862NB-I00, PID2022-136861NB-I00, and PID2022-139296NB-I00, funded by MICIU/AEI/10.13039/501100011033 and the European CNS2023-143600 (MICIU/AEI NextGenerationEU/PRTR); and 2024ICT334 (CSIC). Financial support from the Gobierno de Aragón-Fondo Social Europeo (E07_23R) and the Spanish network OASIS (RED2022-134074-T) is also acknowledged. M.R. gratefully acknowledges the Recherche Médicale (FRM, Fondation pour la SPF202309017545).

Data availability

View Article Online DOI: 10.1039/D5CC04768D

Journal Name

Data supporting this article have been included in the supplementary information (SI). Supplementary information is available. See DOI:

CCDC 2405786 contains the supplementary crystallographic data for complex 3.

Conflicts of interest

There are no conflicts of interest to declare

Notes and references

- K. D. Mjos and C. Orvig, Chem. Rev., 2014, 114, 4540–4563.
- S. Monro, K. L. Colón, H. Yin, J. Roque, P. Konda, S. Gujar, R. P. Thummel, L. Lilge, C. G. Cameron and S. A. McFarland, Chem. Rev., 2019, 119, 797-828.
- Y. Wu, S. Li, Y. Chen, W. He and Z. Guo, Chem. Sci., 2022, 13, 5085-5106.
- B. Kar, U. Das, N. Roy and P. Paira, Coord. Chem. Rev., 2023, 474, 214860.
- J. Sanz-Villafruela, A. Carbayo, M. Martínez-Alonso and G. Espino, Coord. Chem. Rev., 2025, 534, 216572.
- M. Negi, T. Dixit and V. Venkatesh, Inorg. Chem., 2023, 62,
- T. Feng, Z. Tang, J. Karges, J. Shu, K. Xiong, C. Jin, Y. Chen, G. Gasser, L. Ji and H. Chao, Chem. Sci., 2024, 15, 6752-6762.
- J. Kasparkova, V. Novohradsky, J. Ruiz and V. Brabec, Chem.-Bio. Interact., 2024, **392**, 110921.
- F.-X. Wang, M.-H. Chen, Y.-N. Lin, H. Zhang, C.-P. Tan, L.-N. Ji and Z.-W. Mao, ACS Appl. Mater. Interfaces, 2017, 9, 42471-42481.
- 10 J. Sanz-Villafruela, C. Bermejo-Casadesús, G. Riesco-Llach, M. Iglesias, M. Martínez-Alonso, M. Planas, L. Feliu, G. Espino and A. Massaguer, Inorg. Chem., 2024, 63, 19140-19155.
- 11 K. E. De Visser and J. A. Joyce, Cancer Cell, 2023, 41, 374-403.
- 12 M. Redrado, E. Romanos, A. Benedi, G. Canudo-Barreras, I. Marzo, M. C. Gimeno and V. Fernández-Moreira, Inorg. Chem. Front., 2024, 11, 1828-1838.
- 13 L. Wang, J. Karges, F. Wei, L. Xie, Z. Chen, G. Gasser, L. Ji and H. Chao, Chem. Sci., 2023, 14, 1461–1471.
- 14 T. Yoshihara, Y. Yamaguchi, M. Hosaka, T. Takeuchi and S. Tobita, Angew Chem Int Ed, 2012, 51, 4148-4151.
- 15 S. Ladouceur, D. Fortin and E. Zysman-Colman, Inorg. Chem., 2011, 50, 11514-11526.
- 16 T. Yoshihara, S. Murayama, T. Masuda, T. Kikuchi, K. Yoshida, M. Hosaka and S. Tobita, J. Photochem. Photobiol. A: Chem., 2015, **299**, 172-182.
- 17 A. I. Solomatina, K. M. Kuznetsov, V. V. Gurzhiy, V. V. Pavlovskiy, V. V. Porsev, R. A. Evarestov and S. P. Tunik, Dalton Trans., 2020, 49, 6751-6763.
- 18 D.-H. Cai, C.-L. Zhang, Q.-Y. Liu, L. He, Y.-J. Liu, Y.-H. Xiong and X.-Y. Le, Eur. J. Med. Chem., 2021, 213, 113182.
- S. Amézqueta, X. Subirats, E. Fuguet, M. Rosés and C. Ràfols, in Liquid-Phase Extraction, Elsevier, 2020, pp. 183-208.
- 20 M. Redrado, A. Benedi, I. Marzo, A. L. García-Otín, V. Fernández-Moreira and M. C. Gimeno, Chem. A Eur. J., 2021, **27**, 9885-9897.
- 21 S. Fulda, L. Galluzzi and G. Kroemer, Nat. Rev. Drug. Discov., 2010. **9**. 447-464.
- 22 L. Saladin, V. Breton, V. Le Berruyer, P. Nazac, T. Lequeu, P. Didier, L. Danglot and M. Collot, J. Am. Chem. Soc., 2024, **146**, 17456-17473.

Data availability

Data supporting this article have been included in the supplementary information (SI). Supplementary information is available. See DOI:

CCDC 2405786 contains the supplementary crystallographic data for complex 3.